2020 IEEE-RAS 20th International Conference on Humanoid Robots (Humanoids)
July 19-21, 2021. Munich, Germany

2020 IEEE-RAS 20th International Conference on Humanoid Robots (Humanoids) | 978-1-7281-9372-4/21/$31.00 ©2021 IEEE | DOI: 10.1109/HUMANOIDS47582.2021.9555775

MPC-based Locomotion Control of Bipedal Robots with Line-Feet Contact using Centroidal Dynamics.

Gabriel García[1], Robert Griffin[1], and Jerry Pratt[1]

***Abstract*— Recently we have seen a lot of progress done in dynamic locomotion with quadrupedal robots using the Single-Rigid Body Model, which contains simplified dynamics that considers the robot a single "potato". This approach performs poorly when the robot contains heavy links, because those links take a considerable momentum to move and because they also change the overall inertia of the robot. In this paper, we generalize the SRBM using the Centroidal Dynamics model plus an orientation variable, whose dynamics contain the linearized effects of other links' momentum and variable inertia. We are designing this Enhanced Centroidal Dynamics using the Full-Body Dynamics, so the trajectories we obtain are instantaneously dynamically feasible. We show our approach in a full-body dynamic simulation of the MIT Humanoid, a biped with line-feet contact, and we show a simplification in the modeling of the wrenches that can be applied with line-feet.**

I. INTRODUCTION

In general, the locomotion of a bipedal robot is a hard problem to solve from the control perspective. A big limitation of bipedal robots with respect to fixed-base robots, like manipulators, is that the contacts of the robot in the world may be broken depending on conditions like friction or unilateral contact. These constraints prevent the application of any control law at the joint level, because the projection of that control law to the forces applied on the contacts may break them.

This problem has been solved with the consideration of the instantaneous dynamics of the floating base and the forces constrained at each joint [1]. Those instantaneous dynamics are linear and the problem is usually solved with a Quadratic Program optimization (QP) [2], [3], [4], [5]. Those approaches are called in general "Whole-Body Controllers" (WBC) and although the solution is not a simplification, they do not contain any long-term plan for stabilization.

In order to solve the long-term problem, there should be something on top sending reference trajectories to a WBC. References to the joints can be sent (like the local position of the arms), but also task-space trajectories can be sent (such as the trajectory of a swinging foot). More complex tasks can be sent, for example, in [6] authors found that the angular momentum around the Center of Mass of a walking human is very close to zero; so angular momentum equal to zero is a reasonable task to send. At this point, many approaches considering angular momentum equal to zero have emerged, for example, approaches like the Linear Inverted Pendulum [7], [8], Divergent Component of Motion [9], [10], or the Variable-Height Inverted Pendulum [11], [12], [13]. But none of these approaches considers the orientation of the robot. In any case, the question of what are the feasible trajectories given a sequence of contacts and the full-body dynamics (or equivalently, by a whole-body controller) depends on specific equations of the joints [1] [14]. Those equation are given by the linear momentum and the angular momentum, and the dynamics and control of those variables is a research topic called centroidal dynamics [15]. We say that a centroidal trajectory is *dynamically feasible* if it can be generated by a sequence of contacts and their respective friction constraints.

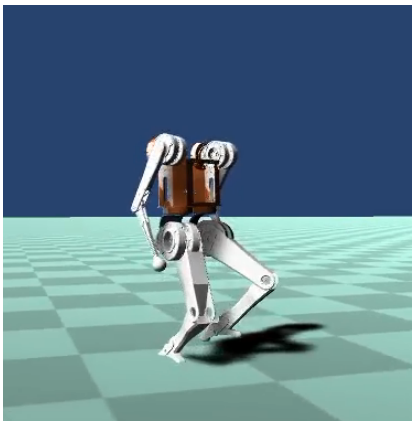

Fig. 1. MIT Humanoid full-body simulation. Turning while walking

There are a few approaches dealing with the angular dynamics of a robot. Direct optimization over the joint variables requires offline computation given the slow solving time [16]. In [17] authors decompose the centroidal dynamics into a convex and a concave part, and they use a QCQP (Quadratically Constrained Quadratic Program) for finding feasible centroidal trajectories. [18] consider trajectories generated with kinematics and dynamically feasible, but they also use a QCQP for the trajectories. The time required for solving a QCQP is greater than the solving time of a common QP, which features only linear constraints. In [19] authors solve for the centroidal dynamics using a QCQP and polynomial curves for the Center of Mass (CoM) and the angular momentum. Although this results in continuous trajectories, they have a limitation of generality: the CoM trajectories have a maximum degree, and in consequence, the number of parameters is limited. The dynamics of the angular momentum are fully linear after a transformation that computes the angular momentum around a fixed point in the world coordinates. This was used in [20] to obtain trajectories with an upper bound minimized in the angular

[1]Authors are with The Florida Institute for Human and Machine Cognition, Pensacola, FL, USA {ggarcia, rgriffin, jpratt}@ihmc.us

momentum with a QP program.

An orientation variable can be added to the Centroidal Dynamics while considering only a single body. This model is called Single-Rigid Body Model (SRBM), and this was done and had successful results in quadruped robots. In [21] and [22], authors used a simplified version of the SRBM to control the orientation of MIT Mini-Cheetah. In [23], [24], [25] authors are focused on the design of heuristics that fix the errors of the performance of the control of the SRBM with non-linear optimization. But there are not generalizations of the SRBM to bipeds yet, especially because bipeds change their inertia depending on the joint configuration and other links take momentum to move. In this paper, we generalize the SRBM to humanoids in an approach based on an "Enhanced Centroidal Dynamics" which considers also an orientation variable for the Floating-Base of the robot.

A. Contributions

The most important contribution of this paper is stated as:

- Provide a model that generates centroidal and orientation trajectories of a robot while considering the effects of variable inertia and the distribution of the angular momentum among the links.

We also show that those trajectories are dynamically feasible trajectories (a WBC solves the problem almost perfectly), we simplify the equation of a Line Contact Wrench Cone instead of two contact points at the feet (which is our case of study) and we implement a contact estimator based on residuals from previous works [26], [27]. We test our results in the locomotion of the MIT Humanoid, shown in Fig. 1.

II. BACKGROUND

A. Mathematical Model

The dynamic equations of a n degree-of-freedom robot

$$H(q)\ddot{q}+\phi(q,\dot{q})=\tau+J(q)^T f, \tag{1}$$

where $q\in\mathbb{R}^n$ represents the joint coordinates, $H(q)\in\mathbb{R}^{n\times n}$ is the inertial matrix, $\phi(q,\dot{q})\in\mathbb{R}^n$ contains the Coriolis and gravitational terms, $\tau\in\mathbb{R}^n$ is the torque applied at each joint, $J\in\mathbb{R}^{3\times n}$ is the geometric Jacobian, and f is a contact force at the feet.

The Centroidal Dynamics of any Multi-body System under multi-contact, line-feet placements holds as:

$$\begin{bmatrix} m\ddot{\mathbf{r}} = m\mathbf{g}+\sum_{i=1}^{n}\mathbf{f}_i \\ \dot{\mathbf{L}} = \sum_{i=1}^{n}(\mathbf{r}_{pi}-\mathbf{r})\times\mathbf{f}_i+\tau_i \end{bmatrix} \tag{2}$$

where:

- m is the mass of the robot
- $\mathbf{r}$ is the position of the CoM
- $\mathbf{g}$ is the gravity vector
- $\mathbf{f}_i$ is the i^{th} ground reaction force
- τ_i is the i^{th} ground reaction torque
- $\mathbf{L}$ is the angular momentum around the CoM
- $\mathbf{r}_{pi}$ is the position of the i^{th} contact

We assume that $\mathbf{r}_{pi}$ is given in time, i.e. the foot placement is already specified ahead of time from a contact sequence generator. Note that there is not a concept of "orientation" yet.

We are going to use an angular momentum with respect to a fixed point instead of respect to the CoM. This will linearize the dynamics (2). We are going to define $L_G = \mathbf{L}+m(\mathbf{r}-\mathbf{r_G})\times\dot{\mathbf{r}}$ where $\mathbf{r_G}$ is a fixed point in the space. Taking time derivative, we have:

$$\dot{L}_G=\sum_{i=1}^{n}((\mathbf{r}_{pi}-\mathbf{r_G})\times\mathbf{f}_i+\tau_i)+(\mathbf{r}-\mathbf{r_G})\times(m\mathbf{g}) \tag{3}$$

B. Variational linearization of $SO(3)$

We are going to perform variations in the dynamics of $SO(3)$ as follows. We have reference functions $R_d(t)\in SO(3)$ and $\Omega_d(t)\in\mathbb{R}^3$ holding:

$$\dot{R}_d = R_d[\Omega_d]_\times \tag{4}$$

where $[\bullet]_\times\in\mathbb{R}^{3\times3}$ and it holds $[a]_\times b = a\times b$. We consider Ω as the real angular velocity of the floating base. The dynamics of the rotation $R\in SO(3)$ of the floating base is:

$$\dot{R} = R[\Omega]_\times \tag{5}$$

We perform a linearization of R around R_d, i.e, $R\approx R_d+\varepsilon\delta R$. We desire R to remain linearly orthogonal, i.e.: $(R_d+\varepsilon\delta R)^T(R_d+\varepsilon\delta R)=I+O(\varepsilon^2)$ which implies:

$$R_d^T\delta R+\delta R^T R_d = 0\rightarrow R_d^T\delta R\in\mathfrak{so}(3) \tag{6}$$

Which means that for some $\eta\in\mathbb{R}^3$ we have:

$$\delta R = R_d[\eta]_\times \tag{7}$$

We apply the variational operator to (5) to obtain a relation between the variation η and the variation of Ω, defined as $\delta\Omega=\Omega-\Omega_d\rightarrow\Omega=\Omega_d+\delta\Omega$:

$$\dot{\delta R} = \delta R[\Omega_d]_\times + R_d[\delta\Omega]_\times$$

We replace $\dot{\delta R}$ with the derivative of (7):

$$\dot{R}_d[\eta]_\times+R_d[\dot{\eta}]_\times = R_d[\eta]_\times[\Omega_d]_\times+R_d[\delta\Omega]_\times$$

$$[\dot{\eta}]_\times = [\eta]_\times[\Omega_d]_\times-[\Omega_d]_\times[\eta]_\times+[\delta\Omega]_\times$$

Using the property $[a\times b]_\times=[a]_\times[b]_\times-[b]_\times[a]_\times$ we finally have:

$$\dot{\eta}=\eta\times\Omega_d+\delta\Omega \tag{8}$$

which is the relation between the variation η and $\delta\Omega$.

III. CONTROL APPROACH

A. Simplified Line Contact Wrench Cone

A common way to write constraints of a line contact is to consider the extremes of that line as two contact points. In this case, the classical (linearized) friction cone is written as:

$$\begin{gathered} -\mu f_{z,i}\le f_{x,i}\le\mu f_{z,i}, \\ -\mu f_{z,i}\le f_{y,i}\le\mu f_{z,i}, \\ 0\le f_{z,i} \end{gathered} \tag{9}$$

for $i=1,2$, which are the indexes of the contact points. Ignoring the last constraint (because it's a consequence of

either, the first or the second row of (9)), we have in total 8 inequalities and 6 variables (3 forces per each point contact). In this subsection, we will simplify those to 6 inequalities and 5 variables.

In [28] a closed form of the equations of the Contact Wrench Cone was presented for the reduction of the number of inequalities for a rectangular planar contact. Here we use those equations for the case when the width of the rectangular foot is zero. We are obtaining a line contact by just evaluating the CWC inequalities from [28]. Thus, we obtain the following constraints in local foot coordinates:

$$|f_x| \leq \mu f_z \tag{10}$$

$$|f_y| \leq \mu f_z \tag{11}$$

$$0 \leq f_z \tag{12}$$

$$|\tau_x| \leq 0 \rightarrow \tau_x = 0 \tag{13}$$

$$|\tau_y| \leq X f_z \tag{14}$$

$$-\mu X f_z + |X f_y - \mu \tau_y| \leq \tau_z \leq \mu X f_z - |X f_y + \mu \tau_y| \tag{15}$$

Where X is the half of the length of the feet. Now we will show that (11) and (14) are a consequence of (15). If (15) holds, then the upper bound of τ_z is automatically greater than the lower bound. Rearranging and using the property $|a+b|+|a-b| = 2\max\{|a|,|b|\}$ we obtain:

$$\max\{|X f_y|, |\mu \tau_y|\} \leq \mu X f_z \tag{16}$$

which implies both:

$$|\tau_y| \leq X f_z \quad and \quad |f_y| \leq \mu f_z \tag{17}$$

This means that (15) implies (11) and (14), so we do not need to write them. Also, the unilateral constraint (12) is a direct consequence of either (10) or (15), so we can safely remove it. Finally, we have the following constraints on the line contact:

$$\begin{bmatrix} |f_x| \leq \mu f_z \\ -\mu X f_z + |X f_y - \mu \tau_y| \leq \tau_z \leq \mu X f_z - |X f_y + \mu \tau_y| \end{bmatrix} \tag{18}$$

Eq. (18) contains 6 inequalities and removing $\tau_x = 0$ from our variables we have only 5 variables $(\tau_y, \tau_z, f_x, f_y, f_z)$.

B. Contact Estimator

The contact estimator is based on a Momentum-based Disturbance Observer in the full-body model and a Jacobian pseudoinverse. We assume that all perturbations come from the line contacts. We present first the dynamics of the observer in discrete time, equivalent to the observer found in [29]. We have the following dynamics:

$$H(q)\ddot{q} + C(q,\dot{q})\dot{q} + G(q) = \tau + J_g(q)^T f_g \tag{19}$$

$H(q)$ must hold: $\dot{H}(q) = C(q,\dot{q}) + C^T(q,\dot{q})$. Defining $\tau_d = J_g(q)^T f_g$ we obtain:

$$\tau_d = \frac{\mathrm{d}(H(q)\dot{q})}{\mathrm{d}t} - C^T(q,\dot{q})\dot{q} + G(q) - \tau \tag{20}$$

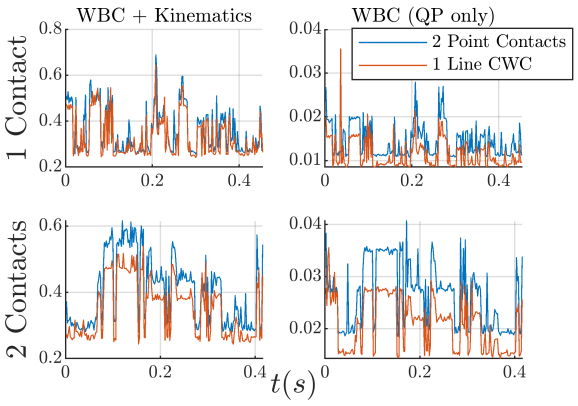

Fig. 2. Solving time using a line contact instead of two point contacts. See Section IV

We use the generalized momentum p as $p = H(q)\dot{q}$ Discretizing the derivative and applying a low pass filter we obtain the following difference equation:

$$\tau_{d,k} = \gamma \tau_{d,k-1} + (1-\gamma)(\frac{p_k - p_{k-1}}{\Delta t} - C_k^T \dot{q}_k + G_k - \tau_k) \tag{21}$$

We require the matrix C^T (or at least $C^T\dot{q}$) for using (21), so we implemented the Coriolis Matrix from [27] which is compatible with Featherstone's Algorithm.

In order to estimate the generalized force f_g from $\tau_d = J_g(q)^T f_g$, we simply use a pseudoinverse $f_{g,k} = J_g(q_k)^{T\dagger}\tau_{d,k}$. This is a solution to the following simplified problem presented in [26]:

$$\begin{aligned} &\mathbb{P}_g : \min_{f_g} \|\tau_{d,k} - J_g(q_k)^T f_g\|_Q^2, \ s.t. \\ &W f_g \leq b \end{aligned} \tag{22}$$

Where W and b encodes the friction constraints on the contacts. For now, this is used to trigger early contact, since locomotion performs poorly when the WBC assumes that it is not in contact and actually it is.

C. Enhanced Centroidal Dynamics Model

Recalling (2), there is a concept of "position" as the double integral of the acceleration $\ddot{\mathbf{r}}$, but there is no concept of "orientation". In this section we will use (2) with a linearized dynamics of the orientation and we will consider the effects of variable inertia and the angular momentum distribution among other links.

In other words, we are going to extend the classical Single Rigid Body Model to a system in which the torso does not dominate in mass or inertia, like in quadrupeds.

In works related to quadrupeds, the angular momentum was directly applied to the torso of a robot. So we have the equality $\mathbf{L} = \mathbf{R}\mathbf{I}_\mathbf{B}\Omega$. We will use the real definition of the angular momentum. We are considering the vector of velocities as $\dot{q} = [\Omega \ \upsilon \ \dot{q}_a]^T$, where Ω and υ are the angular and linear velocity of the floating base respectively, and $\dot{q}_a$ the rest of the joints. The local angular momentum of the system with respect to the floating base can be written as:

$$L_l = I_B(q_a)\Omega + A_l(q_a)\dot{q}_a \tag{23}$$

Where $I_B(q_a)$ and $A_l(q_a)$ come from the Centroidal Momentum Matrix. So the angular momentum with respect to the world can be written as:

$$\mathbf{L} = RL_l = R(I_B(q_a)\Omega + A_l(q_a)\dot{q}_a) \tag{24}$$

Now, we are going to compute the variations of $\mathbf{L}$ with respect to Ω and R. We will not consider the angles q_a as variables in this enhanced centroidal dynamics model, so we are going to consider $\delta q_a = 0$. Otherwise, the system will have an increased number of states than the classic Single Rigid Body Model. We drop the argument q_a in I_B.

$$\delta\mathbf{L} = \delta R(I_B\Omega + A_l(q_a)\dot{q}_a) + RI_B\delta\Omega$$

$$\delta\mathbf{L} = \delta RR^T\mathbf{L} + RI_B\delta\Omega$$

$$\delta\Omega = I_B^{-1}(R^T\delta\mathbf{L} - [\eta]_\times R^T\mathbf{L}) \tag{25}$$

Replacing (25) into (8) we obtain:

$$\dot{\eta} = \eta\times\Omega + I_B^{-1}(R^T\delta\mathbf{L} - [\eta]_\times R^T\mathbf{L}) \tag{26}$$

Reordering:

$$\dot{\eta} = (I_B^{-1}[R^TL]_\times - [\Omega]_\times)\eta + I_B^{-1}R^T\delta\mathbf{L} \tag{27}$$

We will be using the angular momentum around a fixed point G $L_G = \mathbf{L} + m(\mathbf{r}-\mathbf{r_G})\times\dot{\mathbf{r}}$, so we write:

$$\delta\mathbf{L} = \mathbf{L} - L_d = L_G - m(\mathbf{r}-\mathbf{r_G})\times\dot{\mathbf{r}} - L_d \tag{28}$$

We linearize the crossed term as

$$(\mathbf{r}-\mathbf{r_G})\times\dot{\mathbf{r}} \approx (\mathbf{r_d}-\mathbf{r_G})\times\dot{\mathbf{r}} + (\mathbf{r}-\mathbf{r_d})\times\dot{\mathbf{r}}_\mathbf{d} \tag{29}$$

Replacing (29) into (27) we obtain the following dynamics of the variation η:

$$\begin{aligned}\dot{\eta} = (I_{Bd}^{-1}[R_d^TL_d]_\times - [\Omega_d]_\times)\eta + I_{Bd}^{-1}R_d^T(-L_d + m\mathbf{r_d}\times\dot{\mathbf{r}}_\mathbf{d}) \\ + I_{Bd}^{-1}R_d^T(L_G - m([\mathbf{r_d}-\mathbf{r_G}]_\times\dot{\mathbf{r}} - [\dot{\mathbf{r}}_\mathbf{d}]_\times\mathbf{r}))\end{aligned} \tag{30}$$

Eq. (30) is the linearization of the real angular momentum $\mathbf{L}$ of the whole system with respect to the orientation variable η, and it considers the two effects that do not appear in the classical Single-Rigid Body Model: A variable inertia and an angular momentum distribution among the links.

$$\begin{bmatrix} m\ddot{\mathbf{r}} = m\mathbf{g} + \sum_{i=1}^n \mathbf{f}_i \\ \dot{L}_G = \sum_{i=1}^n((\mathbf{r}_{pi}-\mathbf{r_G})\times\mathbf{f}_i + \tau_i) + (\mathbf{r}-\mathbf{r_G})\times(m\mathbf{g}) \\ \dot{\eta} = a_0(t) + a_1(t)\mathbf{r} + a_2(t)\dot{\mathbf{r}} + a_3(t)L_G + a_4(t)\eta \end{bmatrix} \tag{31}$$

Where the functions $a_0(t)\in\mathbb{R}^3$ and $a_i(t)\in\mathbb{R}^{3\times3}$ $\forall i\in[1,4]$ are defined from (30), and they depend only on time and the reference:

$$\begin{aligned} a_0(t) &= I_{Bd}^{-1}R_d^T(-L_d + m\mathbf{r_d}\times\dot{\mathbf{r}}_\mathbf{d}) \\ a_1(t) &= mI_{Bd}^{-1}R_d^T[\dot{\mathbf{r}}_\mathbf{d}]_\times \\ a_2(t) &= -mI_{Bd}^{-1}R_d^T[\mathbf{r_d}-\mathbf{r_G}]_\times \\ a_3(t) &= I_{Bd}^{-1}R_d^T \\ a_4(t) &= I_{Bd}^{-1}[R_d^TL_d]_\times - [\Omega_d]_\times \end{aligned}$$

Eq. (31) is an affine time-varying dynamical system for any centroidal dynamics and it also considers the orientation of the floating base. Note that the dynamics on the variables $\mathbf{r}$, $\dot{\mathbf{r}}$ and L_G are exact, and the dynamics in the orientation has only quadratic errors with respect to the reference.

D. MPC Optimization

In this subsection, we are going to apply (31) to a line-feet biped robot. Let R_{fi} for $i=1,2$ be the rotation matrix that casts vectors from the world to local coordinates of the feet (where the x-component lays on the line-feet). Then we have:

$$R_{fi}\tau_i = \tau_{li} \tag{32}$$

Where τ_{li} represents the torque in local coordinates of the feet. From equation (13) in III-A we know that the x-coordinate of the local torque is 0, i.e. $\tau_{li,x}=0$. We have:

$$\tau_{li} = \begin{bmatrix}\mathbf{0}_{1\times2}\\ \mathbf{I}_{2\times2}\end{bmatrix}\begin{bmatrix}\tau_{liy}\\ \tau_{liz}\end{bmatrix} \tag{33}$$

We define a matrix

$$A_s = \begin{bmatrix}\mathbf{0}_{1\times2}\\ \mathbf{I}_{2\times2}\end{bmatrix} \tag{34}$$

and a reduced torque as $\tau_{lri} = \begin{bmatrix}\tau_{liy}\\ \tau_{liz}\end{bmatrix}$. We have $\tau_{li} = A_s\tau_{lri}$ and using (32) we have the following equality:

$$\tau_i = R_{fi}^TA_s\tau_{lri} \tag{35}$$

We can plug (35) into (31) and we can write this system in matrix form for two feet as:

$$\dot{\mathbf{x}} = A(t)\mathbf{x} + B(t)\mathbf{u} + C(t) \tag{36}$$

where $\mathbf{x} = [\mathbf{r}\ \dot{\mathbf{r}}\ L_G\ \eta]^T$, $\mathbf{u} = [\mathbf{f}_1\ \tau_{lr1}\ \mathbf{f}_2\ \tau_{lr2}]^T$ and the matrices $A(t)$, $B(t)$ and $C(t)$ come from (31):

$$\mathbf{A}(t) = \begin{bmatrix} \mathbf{0}_{3\times3} & \mathbf{I}_{3\times3} & \mathbf{0}_{3\times3} & \mathbf{0}_{3\times3} \\ \mathbf{0}_{3\times3} & \mathbf{0}_{3\times3} & \mathbf{0}_{3\times3} & \mathbf{0}_{3\times3} \\ -m[\mathbf{g}]_\times & \mathbf{0}_{3\times3} & \mathbf{0}_{3\times3} & \mathbf{0}_{3\times3} \\ a_1(t) & a_2(t) & a_3(t) & a_4(t) \end{bmatrix} \tag{37}$$

$$\mathbf{B}(t) = \begin{bmatrix} \mathbf{0}_{3\times3} & \mathbf{0}_{3\times2} & \mathbf{0}_{3\times3} & \mathbf{0}_{3\times2} \\ \frac{1}{m}\mathbf{I}_{3\times3} & \mathbf{0}_{3\times2} & \frac{1}{m}\mathbf{I}_{3\times3} & \mathbf{0}_{3\times2} \\ [\mathbf{r}_{p1}-\mathbf{r_G}]_\times & R_{f1}^TA_s & [\mathbf{r}_{p2}-\mathbf{r_G}]_\times & R_{f2}^TA_s \\ \mathbf{0}_{3\times3} & \mathbf{0}_{3\times2} & \mathbf{0}_{3\times3} & \mathbf{0}_{3\times2} \end{bmatrix} \tag{38}$$

$$\mathbf{C}(t) = \begin{bmatrix} \mathbf{0}_{3\times1} \\ \mathbf{g} \\ -m\mathbf{r_G}\times\mathbf{g} \\ a_0(t) \end{bmatrix} \tag{39}$$

Note that the vector $\mathbf{u}$ contains two torques in local coordinates and three forces in global coordinates. We define an MPC setup as $\mathbb{P}$:

$$\begin{aligned} \mathbb{P}: \min_{\mathbf{x},\mathbf{u}} &\int_0^{t_f} \|\mathbf{x}_\mathbf{H}^*(t)-\mathbf{x}\|_\mathbf{L} + \|\mathbf{u}\|_\mathbf{K}\mathrm{d}t,\ \textbf{s.t.} \\ \dot{\mathbf{x}} &= A(t)\mathbf{x} + B(t)\mathbf{u} + C(t), \\ \mathbf{x}(0) &= \mathbf{x}_0, \\ b(t) &\geq \mathbf{W}(t)\mathbf{R}_{big}\mathbf{u}, \end{aligned} \tag{40}$$

where $\mathbf{x}^*_{\mathbf{H}}(t)$ represents a desired trajectory to track for the centroidal dynamics and the orientation of the floating base, $\mathbf{x}_0$ is the initial state of the robot, $\mathbf{W}(t)$ and $b(t)$ encode the friction restrictions defined in (18), $\mathbf{R}_{big}$ casts the vector u to full local coordinates in order to be able to apply directly the constraints (18).

$$\mathbf{R}_{big} = \text{diag}[\mathbf{R}_{big,1}, \mathbf{R}_{big,2}] \tag{41}$$

where the matrices $\mathbf{R}_{big,i}$ are defined for $i = 1, 2$ as:

$$\mathbf{R}_{big,i} = \begin{bmatrix} R_{fi} & \mathbf{0}_{3\times 2} \\ \mathbf{0}_{2\times 3} & \mathbf{I}_{2\times 2} \end{bmatrix} \tag{42}$$

The MPC setup defined in (40) is written with a direct transcription approach and solved as a QP optimization in a condensed form. The problem is solved as [22], with minor modifications to include the term C.

The dynamics in (40) are discretized as:

$$\mathbf{x}[n+1] = \mathbf{A}[n]\mathbf{x}[n] + \mathbf{B}[n]\mathbf{u}[n] + \mathbf{C}[n] \tag{43}$$

Solving for each $\mathbf{x}[n]$, we can condense the equations to:

$$\mathbf{X} = \mathbf{A}_{qp}\mathbf{x}_0 + \mathbf{B}_{qp}\mathbf{U} + \mathbf{C}_{qp} \tag{44}$$

The resulting cost function in (40) corresponds to:

$$J(\mathbf{U}) = \|\mathbf{A}_{qp}\mathbf{x}_0 + \mathbf{B}_{qp}\mathbf{U} + \mathbf{C}_{qp} - \mathbf{x}^*_{Hv}\|_{\mathbf{L}} + \|\mathbf{U}\|_{\mathbf{K}} \tag{45}$$

where $\mathbf{x}^*_{Hv}$ is the heuristic $\mathbf{x}^*_H$ vertically stacked. We have the QP optimization written as:

$$\begin{gathered} \mathbb{P}_{\mathbb{D}} : \min_{\mathbf{U}} \tfrac{1}{2}\mathbf{U}^{\mathbf{T}}\mathbf{H}\mathbf{U} + \mathbf{U}^{\mathbf{T}}\mathbf{g}, \; s.t. \\ \mathbf{W}_{\mathbf{qp}}\mathbf{U} \leq \mathbf{b}_{\mathbf{qp}} \end{gathered} \tag{46}$$

where $\mathbf{W}_{\mathbf{qp}}$ and $\mathbf{b}_{\mathbf{qp}}$ are built using the friction inequalities from (40) and $\mathbf{H}$ and $\mathbf{g}$ are defined as:

$$\mathbf{H} = \mathbf{2}(\mathbf{B}^{\mathbf{T}}_{\mathbf{qp}}\mathbf{L}\mathbf{B}_{\mathbf{qp}} + \mathbf{K}) \tag{47}$$

$$\mathbf{g} = \mathbf{2}\mathbf{B}^{\mathbf{T}}_{\mathbf{qp}}\mathbf{L}(\mathbf{A}_{\mathbf{qp}}\mathbf{x}_0 + \mathbf{C}_{\mathbf{qp}} - \mathbf{x}^*_{Hv}) \tag{48}$$

The MPC velocities are close to the commanded velocities, as can be seen in Fig. 3. The Floating-Base Orientation performs pretty well with respect to the desired orientation values (plotted in Euler Angles in Fig. 4). In comparison, a common SRBM approach will not track and eventually break roll/pitch safe limits as in "Base MPC" in Fig. 4.

E. Whole-Body Controller

The QP formulation $\mathbb{P}_{\mathbb{D}}$ given in (46) finds desired wrenches to apply at the contacts and trajectories for the CoM position and orientation. The WBC given in [5] is used to track those trajectories with minor modifications to include the efects of the line contact. It is written as:

$$\min_{\delta_{\mathbf{fr}}, \delta_{\mathbf{f}}} \quad {\delta_{\mathbf{fr}}}^T \boldsymbol{Q}_1 \delta_{\mathbf{fr}} + {\delta_{\mathbf{f}}}^T \boldsymbol{Q}_2 \delta_{\mathbf{f}}, \quad s.t. \tag{49}$$

$$\begin{gathered} \mathbf{S_f}(\mathbf{A}\ddot{\mathbf{q}} + \mathbf{b} + \mathbf{g}) = \mathbf{S_f}{\mathbf{J_c}}^T\mathbf{f_r} \\ \ddot{\mathbf{q}} = \ddot{\mathbf{q}}^{cmd} + \begin{bmatrix} \delta_{\mathbf{f}} \\ \mathbf{0}_{n_j} \end{bmatrix} \\ \mathbf{f_r} = {\mathbf{f_r}}^{MPC} + \delta_{\mathbf{fr}} \\ \mathbf{W}\mathbf{R}^T_{big}\mathbf{f_r} \leq \mathbf{b} \end{gathered}$$

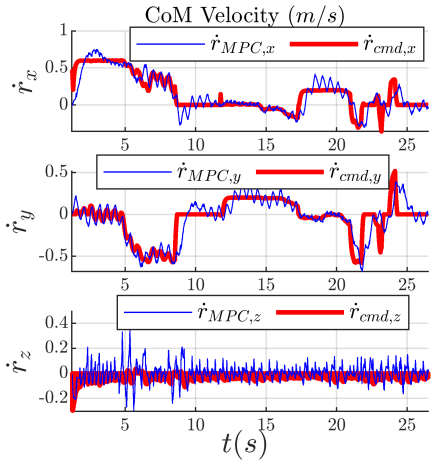

Fig. 3. Commanded CoM velocities vs Resulting CoM velocities MPC

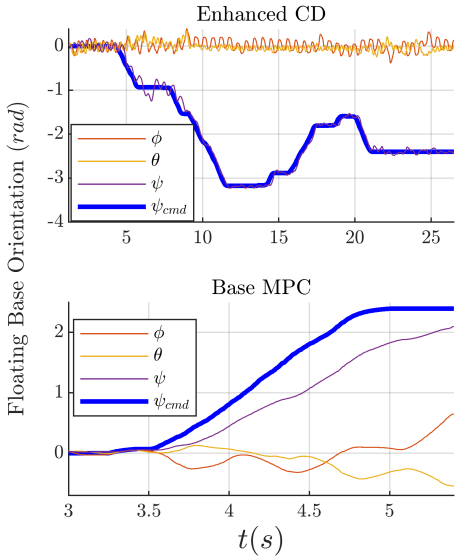

Fig. 4. Commanded RPY orientation of the floating base vs Resulting RPY. Roll ϕ, Pitch θ, Yaw ψ

where $\delta_{\mathbf{fr}}$ and $\delta_{\mathbf{f}}$ are the errors with respect to the MPC solution on the ground reaction force and on the acceleration of the floating base respectively, Q_1 and Q_2 are weights for the errors in the ground reaction force and on the acceleration of the floating base, $\mathbf{A}$, $\mathbf{b}$, $\mathbf{g}$ and $\mathbf{J}^{\mathbf{T}}_{\mathbf{c}}\mathbf{f_r}$ represents the full-dynamics, and $\mathbf{W}$ and $\mathbf{b}$ contains the friction constraints for horizontal terrain, $\mathbf{R}_{big}$ is the matrix defined in (41).

In this setup, the vector $\mathbf{f_r}$ contains not only the forces but also the local torques of the line contact, same as the definition of $\mathbf{u}$ in (36). Thus, the jacobian $\mathbf{J_c}$ must be redefined. Let v_{fi} be the linear velocity and ω_{fi} the angular velocity of the middle point of the i-th foot. Then we have for some jacobian $\mathbf{J}_{v,\mathbf{i}}$:

$$\begin{bmatrix} v_{fi} \\ \omega_{fi} \end{bmatrix} = \begin{bmatrix} \mathbf{J}_{v,\mathbf{i}} \\ \mathbf{J}_{\omega,\mathbf{i}} \end{bmatrix} \dot{q} \tag{50}$$

Recalling (34) and (35), we define a line contact jacobian

as $\mathbf{J_{c,i}} \in \mathbb{R}^{5\times(n_{DoF}+6)}$:

$$\mathbf{J_{c,i}} = \begin{bmatrix} \mathbf{J_{v,i}} \\ A_s^T R_{fi} \mathbf{J_{\omega,i}} \end{bmatrix} \tag{51}$$

and the jacobian $\mathbf{J_c}$ from (49) is just $\mathbf{J_c} = [\mathbf{J_{c,1}}, \mathbf{J_{c,2}}]$.

The vector $\ddot{\mathbf{q}}^{cmd}$ is defined using a strictly prioritized task execution as it is shown in [5] or [30]. The WBC receives tasks and it generates commanded accelerations $\ddot{\mathbf{q}}^{cmd}$. We provide the linear and angular momentum as tasks to the WBC (based on [31]), as follows:

$$\ddot{\mathbf{r}} = \ddot{\mathbf{r}}_d - K_{D,r}(\dot{\mathbf{r}} - \dot{\mathbf{r}}_d) - K_{P,r}(\mathbf{r} - \mathbf{r}_d) \tag{52}$$

$$\dot{\mathbf{L}} = \dot{\mathbf{L}}_d - K_{P,L}(\mathbf{L} - \mathbf{L}_d) \tag{53}$$

where:

$$\mathbf{L}_d = L_{Gd} - m(\mathbf{r_d} - \mathbf{r_G}) \times \dot{\mathbf{r}}_\mathbf{d}$$
$$\dot{\mathbf{L}}_d = \dot{L}_{Gd} - m(\mathbf{r_d} - \mathbf{r_G}) \times \ddot{\mathbf{r}}_\mathbf{d}$$

Note that all the desired values, $\ddot{\mathbf{r}}_d$, $\dot{\mathbf{r}}_d$, $\mathbf{r}_d$, $\dot{\mathbf{L}}_{Gd}$ and $\mathbf{L}_{Gd}$, come directly from the solution of the MPC optimization and they are the centroidal dynamics variables. The orientation η is not directly inserted in the WBC as it is not the integral of the angular momentum, but the desired angular momentum L_d was actually designed to generate a desired orientation. In the next section, to show the power of the present approach, we show results with zero gains in (52) and (53) ($K_{D,r} = K_{P,r} = K_{P,L} = \mathbf{0}$)

IV. RESULTS

The present approach considering the simplified Line Contact Wrench Cone presents a faster solving times compared with the classical 2 point contact approach, as is shown in Fig. 2. For the kinematics, the solver uses the pseudoinverse of the contact jacobians, which in this case has five variables instead of six.

For one line contact, the QP Optimization and the kinematics show an improvement of 6.37% in solving time (average

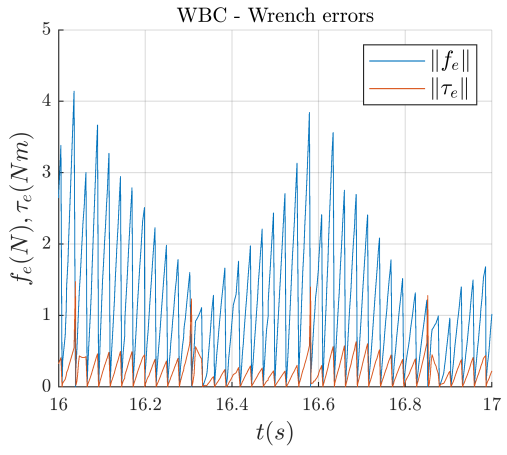

Fig. 5. Force and torque errors between the solutions of MPC and WBC

$\approx 0.33ms$), and the QP itself has an improvement of 20.83% in solving time (average $\approx 0.011ms$).

For double support (two line-contacts), the QP Optimization and the kinematics shows improvement of 13.2% in solving time (average $\approx 0.35ms$), and the QP itself has an improvement of 21.2% in solving time (average $\approx 0.021ms$).

In Fig. 5 and Fig. 6 we can see that the WBC controller performs pretty well given that the centroidal trajectories are feasible. That is the reason why each time that the MPC controller computes a trajectory, the WBC resulting error vanishes to zero. Fig. 5 shows the error between the desired force/torque from the MPC and the resulting force/torque from the QP optimization. These results are obtained while the robot is walking and turning at the same time.

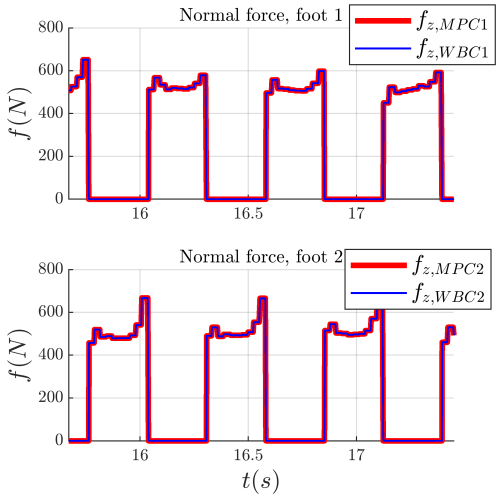

Fig. 6. Desired normal force MPC vs Resulting normal force WBC

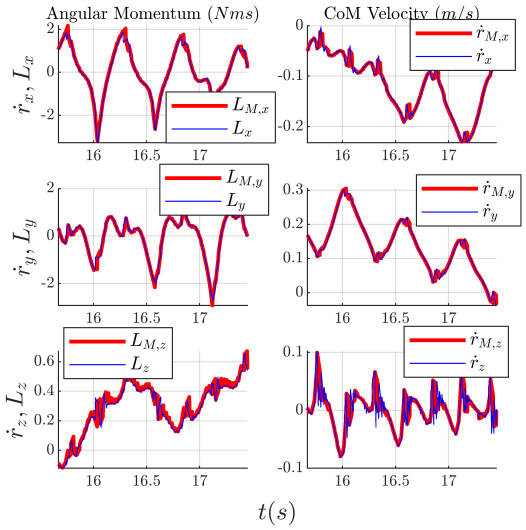

Fig. 7. MPC Centroidal trajectories for the MIT Humanoid

Finally, we can see in Fig. 7 that the WBC perform a good job in tracking the centroidal trajectories. The trajectories sent by the MPC are dynamically feasible so there exist forces that can be applied at each contact to obtain the desired momentum, which implicitly encodes the desired CoM position and Floating-Base orientation of the robot.

V. CONCLUSIONS

We conclude that it is possible to obtain dynamically feasible trajectories for the locomotion of a biped with

an MPC model considering the centroidal dynamics plus the orientation of the floating-base. Those trajectories are dynamically feasible and the WBC solves the problem almost perfectly. While considering a line contact, the use of wrenches results in faster solving time for both, the QP optimization for the WBC and the matrix projections for the inverse kinematics. We have seen that the effects of the angular momentum of links other than the floating-base can be modeled and included in the Enhanced Centroidal Dynamics, so the robot will not suffer from other links having mass and inertia.

VI. ACKNOWLEDGEMENT

The authors would like to thank Dr. Sangbae Kim and the MIT Biomimetics Robotics Lab, and Dr. Donghyum Kim and the Dynamic and Autonomous Robotic Systems (DARoS) Laboratory at UMass Amherst for providing the MIT Humanoid simulation software.

REFERENCES

[1] S. Kajita, F. Kanehiro, K. Kaneko, K. Fujiwara, K. Harada, K. Yokoi, H. Hirukawa. "Resolved momentum control: humanoid motion planning based on the linear and angular momentum". In *Intelligent Robots and Systems (IROS) 2003, IEEE/RSJ International Conference on* , 2003

[2] S. Kuindersma, R. Deits, M. Fallon, A. Valenzuela, H. Dai, F. Permenter, T. Koolen, P. Marion, and R. Tedrake, "Optimization-based locomotion planning, estimation, and control design for the atlas humanoid robot," *Autonomous Robots*, vol. 40, pp. 429–455, Mar 2016.

[3] T. Koolen, T. De Boer, J. Rebula, A. Goswami, and J. Pratt, "Capturability-based analysis and control of legged locomotion, part 1: Theory and application to three simple gait models," *The International Journal of Robotics Research*, vol. 31, no. 9, pp. 1094–1113, 2012.

[4] S. Fahmi, C. Mastalli, M. Focchi and C. Semini, "Passive Whole-Body Control for Quadruped Robots: Experimental Validation Over Challenging Terrain," in *IEEE Robotics and Automation Letters*, vol. 4, no. 3, pp. 2553-2560, July 2019.

[5] D. Kim, J. Di Carlo, B. Katz, G. Bledt, and S. Kim "Highly Dynamic Quadruped Locomotion via Whole-Body Impulse Control and Model Predictive Control," in *arXiv preprint arXiv:1909.0658*, Sep 2019

[6] H. Herr and M. Popovic. "Angular momentum in human walking". Journal of Experimental Biology, 211(4):467–481, 2008.

[7] S. Kajita and K. Tani. "Study of dynamic biped locomotion on rugged terrain-derivation and application of the linear inverted pendulum mode". In *Robotics and Automation (ICRA), 1991 IEEE International Conference on*, vol. 2, pp. 1405-1411, 1991.

[8] J. Pratt, J. Carff, S. Drakunov, and A. Goswami. "Capture Point: A Step toward Humanoid Push Recovery". In *Proceedings of the IEEE-RAS/RSJ International Conference on Humanoid Robots*, pp. 200-207, 2006.

[9] J. Englsberger, C. Ott, M.A. Roa, A. Albu-Schffer, G. Hirzinger. "Bipedal walking control based on capture point dynamics". In *Intelligent Robots and Systems (IROS) 2011, IEEE/RSJ International Conference on*, 2011

[10] J. Englsberger, G. Mesesan, C. Ott. "Smooth trajectory generation and push-recovery based on divergent component of motion". In *Intelligent Robots and Systems (IROS) 2017, IEEE/RSJ International Conference on*, 2017

[11] T. Koolen, M. Posa and R. Tedrake. "Balance control using center of mass height variation: limitations imposed by unilateral contact". In *Humanoid Robots (Humanoids), 2016 IEEE-RAS 16th International Conference on*, pp. 8-15, 2016

[12] S. Caron, A. Escande, L. Lanari, and B. Mallein. "Capturability based analysis, optimization and control of 3d bipedal walking". In *Robotics and Automation (ICRA) 2018, IEEE-RAS International Conference on*, 2018

[13] S. Caron and B. Mallein, "Balance control using both ZMP and COM height variations: A convex boundedness approach", in *Robotics and Automation (ICRA), 2018 IEEE International Conference on*, May 2018.

[14] H. Hirukawa, S. Hattori, K. Harada, S. Kajita, K. Kaneko, F. Kanehiro, K. Fujiwara, and M. Morisawa, "A universal stability criterion of the foot contact of legged robots-adios zmp," in *Robotics and Automation (ICRA), 2006 IEEE International Conference on*, 2006, pp. 1976–1983.

[15] David E. Orin, Ambarish Goswami, and Sung-Hee Lee. "Centroidal dynamics of a humanoid robot". *Autonomous Robots*, (September 2012):1–16, jun 2013.

[16] H. Dai, A. Valenzuela, and R. Tedrake. "Whole-Body Motion Planning with Centroidal Dynamics and Full Kinematics." in *Humanoid Robots (Humanoids), 2014 IEEE-RAS 14th International Conference on*, 2014

[17] B. Ponton, A. Herzog, S. Schaal, and L. Righetti, "A convex model of humanoid momentum dynamics for multi-contact motion generation," in *Humanoid Robots (Humanoids), 2016 IEEE-RAS 16th International Conference on*, 2016.

[18] A. Herzog, S. Schaal, and L. Righetti, "Structured contact force optimization for kino-dynamic motion generation," in *Intelligent Robots and Systems (IROS), 2016 IEEE/RSJ Int. Conference on*, 2016, pp. 2703–2710.

[19] P. Fernbach, S. Tonneau, and M. Tax, "CROC: Convex resolution of Centroidal Dynamics trajectories to provide a feasibility criterion for the multi contact planning problem," in *Intelligent Robots and Systems (IROS), 2018 IEEE/RSJ International Conference on*, Oct 2018.

[20] H. Dai and R. Tedrake. "Planning robust walking motion on uneven terrain via convex optimization", in *Humanoid Robots (Humanoids), 2016 IEEE-RAS 16th International Conference on*, 2016

[21] B. Katz, J. Di Carlo, and S. Kim. "Mini Cheetah: A Platform for Pushing the Limits of Dynamic Quadruped Control", in *Robotics and Automation (ICRA), 2019 IEEE-RAS International Conference on*, 2019

[22] J. Di Carlo, P. Wensing, B. Katz, G. Bledt, and S. Kim. "Dynamic Locomotion in the MIT Cheetah 3 Through Convex Model-Predictive Control", in *Intelligent Robots and Systems (IROS), 2018 IEEE/RSJ International Conference on*, 2018

[23] G. Bledt, P. Wensing and S. Kim. "Policy-regularized model predictive control to stabilize diverse quadrupedal gaits for the MIT cheetah", in *Intelligent Robots and Systems (IROS), 2017 IEEE/RSJ International Conference on*, 2017

[24] G. Bledt, and S. Kim. "Implementing Regularized Predictive Control for Simultaneous Real-Time Footstep and Ground Reaction Force Optimization", in *Intelligent Robots and Systems (IROS), 2019 IEEE/RSJ International Conference on*, 2019

[25] G. Bledt, and S. Kim. "Extracting Legged Locomotion Heuristics with Regularized Predictive Control", to Appear in *Robotics and Automation (ICRA), 2020 IEEE-RAS International Conference on*, 2020

[26] L. Manuelli and R. Tedrake, "Localizing external contact using proprioceptive sensors: The Contact Particle Filter," 2016 IEEE/RSJ International Conference on Intelligent Robots and Systems (IROS), Daejeon, 2016, pp. 5062-5069, doi: 10.1109/IROS.2016.7759743.

[27] S. Echeandia, and P. Wensing "Numerical Methods to Compute the Coriolis Matrix and Christoffel Symbols for Rigid-Body Systems", in *arXiv preprint arXiv:2010.01033*, Oct 2020

[28] S. Caron, Q.-C. Pham, and Y. Nakamura, "Stability of surface contacts for humanoid robots: Closed-form formulae of the contact wrench cone for rectangular support areas," in *Robotics and Automation (ICRA), 2015 IEEE International Conference on*, 2015.

[29] G. Bledt, P. M. Wensing, S. Ingersoll and S. Kim, "Contact Model Fusion for Event-Based Locomotion in Unstructured Terrains", in *Robotics and Automation (ICRA), 2018 IEEE International Conference on*, Brisbane, QLD, 2018, pp. 4399-4406, doi: 10.1109/ICRA.2018.8460904

[30] D. Kim, S. Jorgensen, J. Lee, J. Ahn, J. Luo, and L. Sentis, "Dynamic Locomotion For Passive-Ankle Biped Robots And Humanoids Using Whole-Body Locomotion Control," *arXiv.org*, Jan. 2019.

[31] P. Wensing and D. Orin. "Improved computation of the humanoid centroidal dynamics and application for whole-body control." *International Journal of Humanoid Robotics*, page 1550039, 2015.